

## Simulation of Sloshing Effect on Vessel Motions by Using MPS (Moving Particle Simulation)

K.S. Kim<sup>1</sup>, B.H. Lee<sup>2</sup>, M.H. Kim<sup>1</sup> and J.C. Park<sup>3</sup>

**Abstract:** The coupling and interactions between vessel motion and inner-tank sloshing are investigated by a potential-CFD (Computational Fluid Dynamics) hybrid method in time domain. Potential-theory-based 3D diffraction/radiation panel program is used to obtain the hydrodynamic coefficients and wave forces for the simulation of vessel motion in time domain. The liquid sloshing in tanks is simulated in time domain by using the improved Moving Particle Simulation (PNU-MPS) method and it is validated through comparison against sloshing experiments. The calculated sloshing tank forces and moments are applied to the vessel-motion simulation as excitation forces and moments. The updated ship motion, which is influenced by sloshing-induced tank forces, is in turn inputted to the MPS system as forced motions. For the verification of the coupling, a barge-type FPSO hull with two partially filled inner tanks is selected and the numerically simulated results correlate well against the measurements done by MARIN for various fill ratios. It is seen both in prediction and experiment that the roll RAOs(Response Amplitude Operators) are sensitive to the amount of liquid cargo and can be increased by a factor of 2 or 3 in some wave frequency range compared to the bare-hull or rigid-cargo cases. It is also shown that the nonlinear sloshing effects can alter the vessel-motion characteristics in relatively high waves with the peak period close to sloshing natural frequencies.

**Keywords:** MPS, Ship and liquid tank interaction, CFD, Meshless, Nonlinear Sloshing effect, Coupled dynamic analysis; fill ratio, Navier-Stokes solver, Time-domain potential-viscous hybrid method.

---

<sup>1</sup> TAMU, College Station, TX, U.S.A.

<sup>2</sup> Hyundai Heavy Industry, Ulsan, republic of Korea

<sup>3</sup> PNU, Busan, republic of Korea

## 1 Introduction

Tracking the history of ship-motion analysis, the effects of inner free surface have been usually ignored due to the unavailability of well-established vessel-motion/liquid-sloshing coupled dynamic analysis computer programs. However, the coupling effects can no longer be neglected due to the continuous increase of liquid-tank size in recently-built LNGCs (Liquefied Natural Gas Carriers) and LNG-FPSO (Floating Production Storage Offloading)/FSRU (Floating Storage Re-gasification Unit). It is particularly so when two floating units are operated in close proximity to each other, such as side-by-side LNG-offloading arrangement, in which the hydrodynamic interactions may further increase the liquid sloshing motions and vice versa.

The coupling between vessel motion and liquid sloshing has been studied in time domain by Kim, Shin, Kin, and Yue (2003) and Kim, Nam, Kim, and Kim (2007) and Lee, Kim, Lee, Kim, and Kim (2007) and Lee and Kim (2010) by using the potential-theory-based ship-motion program and 2-D/3-D viscous FDM (Finite Difference Method) sloshing codes. Cho, Hong, Kim, and Park (2007) studied the sloshing-motion coupling effects including two-body interactions in beam waves with a 2-D tank-sloshing CFD code. Lee and Kim (2008) solved the similar two-floating-body problem in side-by-side arrangement by using a 3-D tank-sloshing FDM code.

In the previous studies mentioned above, the CFD codes were limited to non-violent liquid motions without overturning or splashing. So, they were not directly applicable when ship motions are pretty large to generate more violent liquid-sloshing motions. In this regard, a new CFD code based on improved mesh-less MPS (Moving Particle Simulation) method is implemented to solve the liquid-sloshing/vessel-motion interactions with a wide variety of liquid motions including overturning and splashing.

The original MPS method was proposed by Koshizuka, Tamako, and Oka (1996) for incompressible flows. In the original MPS method, however, there were several defects including non-optimal algorithms of source term, gradient/collision models, and search of free-surface particles, which led to less-accurate fluid motions and non-physical pressure fluctuations, as pointed out by authors (Lee, Park and Kim (2010); Hwang, Lee and Park (2010)) and Gotoh (2009).

In the present study, a new MPS method developed by authors Lee, Park and Kim (2011) is used to better simulate more violent liquid sloshing motions and the corresponding excitations and impact loading. The performance and capability of the new MPS method are demonstrated by the comparison with sloshing experiments conducted by Kishlev, Hu, and Kashiwagi (2006). The CPU time is also significantly reduced compared to the original MPS method by using more effective al-

gorithms especially when a large number of particles are involved.

By combining the developed MPS method for sloshing with the time-domain potential-based ship motion program, the vessel-motion and liquid-sloshing interactions can be more accurately simulated for highly nonlinear liquid motions including overturning and splashing. The accuracy of the time-domain ship-motion/mooring fully-coupled dynamics program CHARM3D developed by authors has extensively been verified against experimental and field data [e.g. Kim, Ran, and Zheng (2001); Kim, Koo, Mercier, and Ward (2005); Koo and Kim (2005); Kim and Zhang (2009)]. The developed ship-motion and sloshing-motion simulation programs are coupled in time domain by kinetic and dynamic relations i.e. ship motions first excite the tank motions and the sloshing-induced loads next influence ship motions. Then, the updated ship motions are inputted again for sloshing simulations. The dynamic coupling, therefore, has to be solved simultaneously at each time step with exchanged and updated inputs. To validate the developed coupled program, the calculated ship motion RAOs with partially filled sloshing tanks are compared against the model-test results by MARIN as a part of SALT JIP [Gaillard, Ledoux and Lynch (2004)].

## 2 Ship-Motion Simulation in Time Domain

All the hydrodynamic coefficients were calculated in the frequency domain by using the 3D diffraction/radiation panel program [Lee, Newman, Kim, and Yue (1995); Lee (1991)]. The corresponding forces were converted to those for time domain by using Fourier transform including convolution integral, as shown in Eq. 1

$$\mathbf{F}_R = -\mathbf{M}(\infty)\ddot{\zeta} - \int_{-\infty}^t \mathbf{R}(t-\tau)\dot{\zeta}(\tau)d\tau \quad (1)$$

where  $M(\infty)$  is added mass at infinite frequency and the convolution integral represents the force on the body from the waves generated by body motion prior to time  $t$ .  $M(\infty)$  can be obtained from

$$M^a(\infty) = M^a(\omega) + \int_0^{\infty} \mathbf{R}(t) \frac{\sin(\omega t)}{\omega} dt \quad (2)$$

where  $M^a(\infty)$  is the added mass at frequency  $\omega$ .  $R(t)$  in Eq.1 is retardation function or time memory function which is related to the frequency-domain solution of the radiation problem.  $R(t)$  can be written as

$$\mathbf{R}(t) = \frac{2}{\pi} \int_0^{\infty} \mathbf{C}(\omega) \cos(\omega t) d\omega \quad (3)$$

where

$$C(\omega) = 2\gamma\sqrt{\{M + M^a(\omega)\}K} \tag{4}$$

is the radiation damping coefficients at respective frequencies,  $K$  is restoring matrix, and  $\gamma$  is the damping ratio. The corresponding retardation function has to be calculated for each of the 6x6 radiation damping coefficients. Then the ship motions can be calculated at each time step from

$$[M + M^a(\infty)]\ddot{\zeta} + \int_{-\infty}^t \mathbf{R}(t - \tau)\dot{\zeta}(\tau)d\tau + \mathbf{K}\zeta = \mathbf{F}(t) \tag{5}$$

Where  $F(t)$  includes all kinds of external forces. In the present paper, wind and current loads are not considered, so the external forces consist of wave forces and hull viscous drag forces.

$$\vec{F}_{ext}(t) = \vec{F}_w(t) + \vec{F}_{hv}(t) \tag{6}$$

### 3 Sloshing Simulation by PNU-MPS

#### 3.1 Governing Equations

To simulate liquid sloshing inside the inner tanks, the newly developed MPS method (called PNU-MPS from this point on) is employed. For the MPS, the continuity (Eq.7) and Navier-Stokes (Eq.8) equations are used as the governing equations.

$$\frac{D\rho}{Dt} = 0 \tag{7}$$

$$\frac{D\vec{u}}{Dt} = -\frac{1}{\rho}\nabla P + \nu\nabla^2\vec{u} + \vec{F} \tag{8}$$

where  $\rho$  is the density,  $t$  the time,  $\vec{u}$  the velocity vector,  $\nabla$  the gradient,  $P$  the pressure,  $\nu$  the kinematic viscosity, and  $\vec{F}$  the external force.

The left-hand side of Navier-Stokes equation (Eq. 8) is directly calculated by Lagrangian approach. The right-hand sides consist of pressure gradient, viscous, and external-force terms. For MPS simulation, all terms with differential operators should be replaced by the particle interaction models.

#### 3.2 Kernel Function

Continuous fluid can be represented by the physical quantities of coordinates, mass, velocity components, and pressure for particles. The particle interactions in the

MPS method are based on a kernel function. In this study, the following kernel function is employed:

$$w(r) = \begin{cases} \left(1 - \frac{r}{r_e}\right)^3 \left(1 + \frac{r}{r_e}\right)^3 & (0 \leq r < r_e) \\ 0 & (r_e < r) \end{cases} \quad (9)$$

The distance between two particles is  $r$  and  $r_e$  represents the effective range of particle interactions. The kernel becomes zero when  $r > r_e$ . Since the area covered with this weight function is bounded, a particle interacts with a finite number of neighboring particles. The above kernel tends to be more robust and gives more reasonable interaction models [Lee, Park and Kim (2011)] than that used in the original MPS method [Koshizuka, Tomako and Oka (1996)].

### 3.3 Gradient Model

The gradient vector between the two particles  $i$  and  $j$  possessing scalar quantities  $\varphi_i$  and  $\varphi_j$  at coordinates  $r_i$  and  $r_j$  is defined by  $(\varphi_j + \varphi_i)(r_j - r_i)/|r_j - r_i|^2$  considering the action and reaction between two particles. The gradient vector at the particle  $i$  is given by the weighted average of these gradient vectors (Toyota, Akimoto and Kubo, 2005):

$$\langle \nabla \varphi \rangle_i = \frac{d}{n^0} \sum_{i \neq j} \left[ \frac{\varphi_j + \varphi_i}{|\vec{r}_j - \vec{r}_i|^2} (\vec{r}_j - \vec{r}_i) w(|\vec{r}_j - \vec{r}_i|) \right] \quad (10)$$

Where  $d$  is the number of space dimensions and  $n^0$  is the particle number density fixed for incompressibility in the initial condition of particle arrangement. The particle number density is calculated by the following equation.

$$n_i = \sum_{i \neq j} w(|\vec{r}_j - \vec{r}_i|) \quad (11)$$

The fluid density is proportional to the particle number density.

### 3.4 Diffusion Model

Laplacian ( $\nabla^2$ ), the mathematical operator has a meaning of diffusion. The diffusion of  $\varphi$  at particle  $i$  is described in MPS by

$$\nabla^2 \varphi = \frac{2d}{\lambda} (\varphi_j - \varphi_i) w(|r_j - r_i|) \quad (12)$$

$$\lambda = \frac{\sum_{j \neq i} w(|\vec{r}_j - \vec{r}_i|) |r_j - r_i|^2}{\sum_{j \neq i} w(|\vec{r}_j - \vec{r}_i|)} \cong \frac{\int_V w(r) r^2 dv}{\int_V w(r) dv} \tag{13}$$

where  $\lambda$  is the parameter by which the variance increase is equal to that of the analytical solution. The Laplacian can be modeled by distribution of a physical value from a particle to its neighboring particles by use of the kernel function. The model is conservative since the quantity lost by particle  $i$  is only obtained by the neighboring particle  $j$ .

### 3.5 Incompressibility Model

If the mass of particles is the same for all fluid particles, the fluid density is proportional to particle number density. MPS uses the algorithm of incompressible fluid which is similar to SMAC (Simplified Marker-and-Cell) in grid system. In each time step, there are two stages. In the first step, the explicit step, the intermediate velocity component  $\vec{u}_i^*$  and coordinates  $\vec{r}_i^*$  of particle are obtained by solving diffusion, external forces, and convection terms. The intermediate coordinate  $\vec{r}_i^*$  can be written with intermediate velocity  $\vec{u}_i^*$  and coordinate  $\vec{r}_i^n$  at time  $n$ .

$$\vec{r}_i^* = \vec{r}_i^n + \Delta t \vec{u}_i^* \tag{14}$$

The movement of particle in Eq. 13 is equivalent to the calculation of advection term in grid system. The intermediate particle density number  $\vec{u}_i^*$  can be obtained by using the calculated intermediate coordinate.

In the second stage, implicit stage, the Poisson equation for pressure is calculated implicitly by using the following source equation, which is suggested by Tanaka and Masunaga (2008):

$$\nabla^2 P_i = (1 - \gamma) \frac{\rho}{\Delta t} \nabla \cdot \vec{u}_i^* + \gamma \frac{\rho}{\Delta t^2} \frac{n^0 - n_i^n}{n^0} \tag{15}$$

The blending parameter  $\gamma$  of the right-hand side of (Eq. 14) is a rate of incompressibility and is less than 1.0. The range of  $0.01 < \gamma < 0.1$  looks reasonable from numerical experiments. The left-hand side of (Eq.14) is discretized by the Laplacian model (Eq.12).

Finally, we have simultaneous equations expressed by a linear symmetric matrix and they are solved by iteration method. In the present study, the CG (Conjugate Gradient) method is employed as the iterative solver.

After updating the pressure field, the velocity correction  $\vec{u}'_i$  is calculated by the following equation:

$$\vec{u}'_i = -\frac{\Delta t}{\rho} \langle \nabla P^{n+1} \rangle \quad (16)$$

Finally, the velocity components and coordinates of particles in the  $(n+1)$ -th time step are calculated from the following equations:

$$\vec{u}_i^{n+1} = \vec{u}_i^n + \vec{u}'_i \quad (17)$$

$$\vec{r}_i^{n+1} = \vec{r}_i^n + \Delta t \vec{u}_i' \quad (18)$$

### 3.6 Boundary Condition

The kinematic and the dynamic boundary conditions are imposed as free-surface boundary conditions. The kinematic condition can be directly satisfied by the moving particles on the free surface. In the present method, it is straightforward to track the free surface particles, because the location of the free surface is easily obtained as a result of the full Lagrangian treatment of particles.

In the free surface region, the particle density is decreased, due to the comprisal of the air region. Thus, on the free surface, the following simple condition can be used:

$$\langle n \rangle_i^* = \beta_1 n^0 \quad (19)$$

Where  $\beta_1$  is a parameter below 1.0. In the present simulations, 0.97 is selected. By using the free surface boundary condition, the fragmentation and the coalescence of fluid can be simulated. Free surface particles are easily detected with the free surface parameter  $\beta_1$ .

The dynamic free surface condition is satisfied by taking the atmospheric pressure on the free surface particles. This condition is transformed into the procedure to solve Poisson Equation (Eq. 14).

For the wall boundary condition, the wall particles are set along the solid boundary. Dummy particles are placed inside the solid wall not to be identified as free-surface particles. The wall particles directly contact with both fluid particles and dummy particles. They are employed in the pressure calculation to avoid the concentration of particles near the wall. To satisfy no-slip condition, the wall particles have zero velocity. The velocity of dummy particles is considered in the same manner as the dummy cells in the grid method.

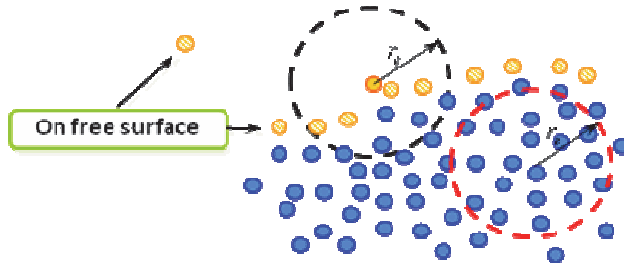


Figure 1: Free-surface model of MPS method

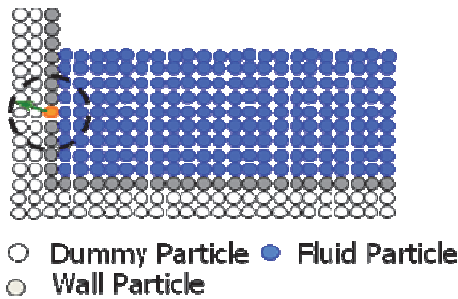


Figure 2: Arrangement of particles around the wall

#### 4 Coupling ship motion and sloshing

In order to couple the ship motion and liquid sloshing, sloshing force vector is added to the right-hand side of Eq.5 as additional external force. The right-hand side of Eq.5 can then be written as follows:

$$\vec{F}(t) = \vec{F}_{ext}(t) + \vec{F}_{slosh}(t) \quad (20)$$

The sloshing force consists of inertia force and interaction force of the liquid.

$$\vec{F}_{slosh}(t) = \vec{F}_{int}(t) + [m_{\text{tank},ij}] \frac{\partial^2 \tilde{\zeta}}{\partial t^2} \quad (21)$$

The interaction force  $\vec{F}_{int}(t)$  contributes to the added-mass term by dynamic pressure and restoring term by hydrostatic pressure. Due to the sloshing liquid motion, the distribution of mass inside the tank and the corresponding mass moment of inertia are constantly changing with time. The effect can be included in the current time-domain simulation.

## 5 Numerical Examples and Discussions

### 5.1 Validation of Sloshing CFD (PNU-MPS)

Let us first consider the water sloshing problem inside a 2D rectangular tank driven by a harmonic oscillator. The simulation results are compared with experimental results of Kishev, Hu, and Kashiwagi (2006). The tank width and height are 0.6(m) and 0.3(m), respectively. The water depth is  $h=0.12$ (m). The tank is forced to move sinusoidally in the horizontal direction with amplitude  $A=0.05$ (m) and period  $T=1.3$ s. The total number of particles used for the simulation is 4000, among which fluid particles are 3000.

Fig. 3a shows the wall-pressure time histories at  $h/6$  below the mean water level. The original MPS, PNU-MPS, and experimental results are shown. The pressure by original MPS method shows non-physical high oscillations. On the other hand, the present PNU-MPS method produces more stable and reasonable pressure field and compares much better against the experimental values than the original MPS method. From this example, it is confirmed that the PNU-MPS correctly simulates the dynamic pressure on tank walls caused by liquid sloshing motions. Fig.3b also presents the free-surface snap shots for three different time frames and it shows that the sloshing patterns at each time step are also very well predicted by the present PNU-MPS method.

### 5.2 Validation of Ship Motion Simulation with/without Sloshing

In the present examples, winds and currents are not considered in order to investigate the dynamic coupling effect between vessel and sloshing motions due to waves at different filling levels of sloshing tank. Table 1 shows the simulation conditions. The wave heading we considered is beam-sea condition. Under this condition, it can be assumed that the liquid sloshing motion is uniform in the longitudinal direction so that 2D sloshing program can be used for more time-effective simulations. Significant wave height, peak period, and enhancement parameter  $\gamma$  of a JONSWAP spectrum are selected as below. Additionally, the filling levels of sloshing tanks are 18%, 37%, and 56% of tank height as the same conditions used in the MARIN experiment.

In this paper, the performance of the developed vessel-motion/liquid-sloshing coupled dynamics program is tested through comparison with the LNG-FPSO experimental results performed by MARIN as a part of SALT-JIP. As shown in Fig.4(a), the FPSO has two rectangular tanks and they are partially filled with fresh water with different filling ratios. Soft springs are used to prevent the drift of LNG-FPSO in waves in the experiment and the same condition is applied in the numerical simulations.

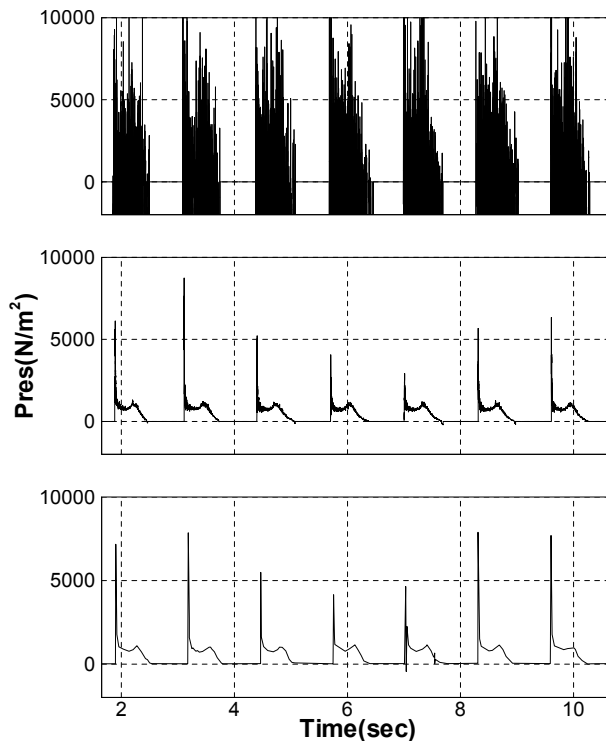


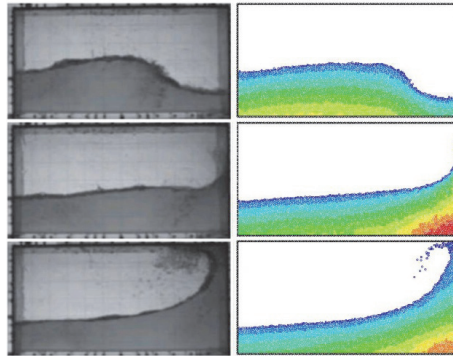
Figure 3a: Comparison of pressure profiles from top to bottom, original MPS, PNU-MPS and experiment. ( $T=1.3\text{sec}$ )

Table 1: Simulation Conditions

Wind	N/A	
Current	N/A	
Wave	Heading	90 Degree (beam)
	Significant Height	5.0 m
	Peak period	12 sec
	$\gamma$ of JONSWAP spectrum	3.3
Filling Level	18%, 37%, 56%	

In the numerical simulation, the hydrodynamic coefficients and linear/drift wave forces can be obtained by using a panel-based 3D diffraction/radiation program, WAMIT [Lee (1995)]. The panels generated are shown in Fig.4(b). The total number of panels for this barge-type FPSO hull is 2375.

The two tanks inside the MARIN-FPSO are shown in Fig.4a and their dimensions



a) Experiment (b) PNU-MPS.

Figure 3b: Comparison of free-surface profiles between experiment and PNU-MPS. From top to bottom, times are  $0.1T$ ,  $0.2T$  and  $0.3T$ .

are summarized in Tab.2. The principal particulars of the MARIN-FPSO and mooring system are given in Tab.3. The hull is designed to be barge type, and the external mooring stiffness is modeled by linear springs for surge, sway, and yaw modes, as used in the experiment.

First, let us consider the case of ship motions without liquid tanks. This simpler case has to be validated against experiments before considering more complicated vessel-motion/liquid-sloshing interaction problems. The infinite water depth condition (wave length  $< 2h$ ) is used, as Marin experiment. Fig.5 shows measured and predicted RAOs with dry tanks (Response Amplitude Operators) for beam (90-degree) wave heading. The predicted RAOs obtained from time-domain simulations correlate well with the MARIN experimental data. On the other hand, the frequency-domain linear-analysis results over-predict the roll RAO near its natural frequency. In the time-domain simulations, the hull viscous drag forces provide additional roll damping to better correlate against the experimental data near the roll natural frequency. The hull viscous drag forces are obtained by using the Morison equation with equivalent viscous plates. Since both the sloshing dynamics and vessel motions with dry tanks are independently verified against respective experimental results, we next consider their coupled dynamics combined in the time-domain simulations.

From this point on, the coupling effects of vessel motion and liquid sloshing are presented. Before presenting the series of representative results, some numerical sensitivity and reliability for the present coupling problem are checked. Typically, the time step used for PNU-MPS is much smaller than that used for vessel-motion

simulations. In this regard, to save the computational time, the vessel-motion time step may be larger than the MPS time step. However, when the sloshing motion is violent, the impact loading on the tank wall can occur in a very short time scale and it can cause non-trivial transient effects. In this case, if the coupling time step is too large, it cannot capture the sloshing impact loading. In this regard, we did some convergence test with varying coupling time steps. It is seen that the results converge satisfactorily for the time steps smaller than MPS time step=0.01s and CHARM3D time step=0.02s. Therefore, MPS time step=0.005s and CHARM3D time step=0.02s are used for the ensuing results. In case of the liquid sloshing motions, nonlinearity and breaking are involved and the sloshing induced loads and the resulting vessel responses may depend on simulation time length. In this regard, we check the sensitivity with varying the simulation time from 1000s to 2500s. It is seen that the differences between them are within 4% after 1500s. For the ensuing results, the simulation-time length is 1800s, which is about the same as that of the experiment for fair comparison. In the beginning of ship-motion simulation, the environmental loading is gradually applied from zero to the actual value within the ramping period (200s) to suppress the transient responses as much as possible in the subsequent times. The response data during the ramping period is not used for the RAO calculations.

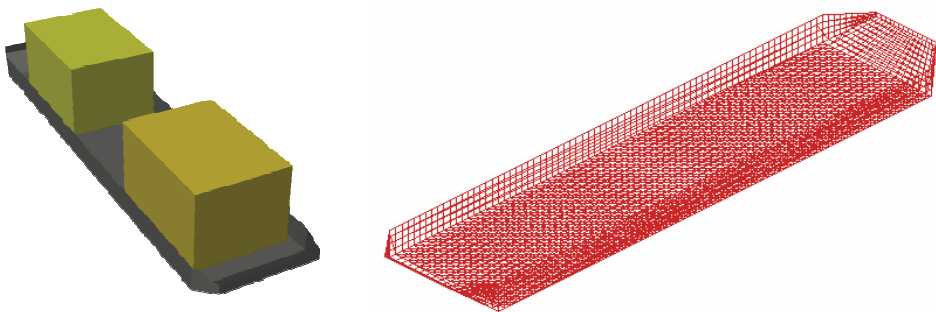


Figure 4: (a) Model of MARIN-FPSO with Sloshing Tanks (b) Model for Panel Method

Fig.6 shows a series of snap-shots of the simulated free-surface profiles and pressure distribution inside the 18%-filled liquid tank for the given wave condition. It is seen that the inner-liquid motions are not so violent for the given environmental condition.

As an independent check for the CFD sloshing simulations, we used the grid-based FDM N-S Solver by ABS called ABSLO3D. Its free-surface treatment is based

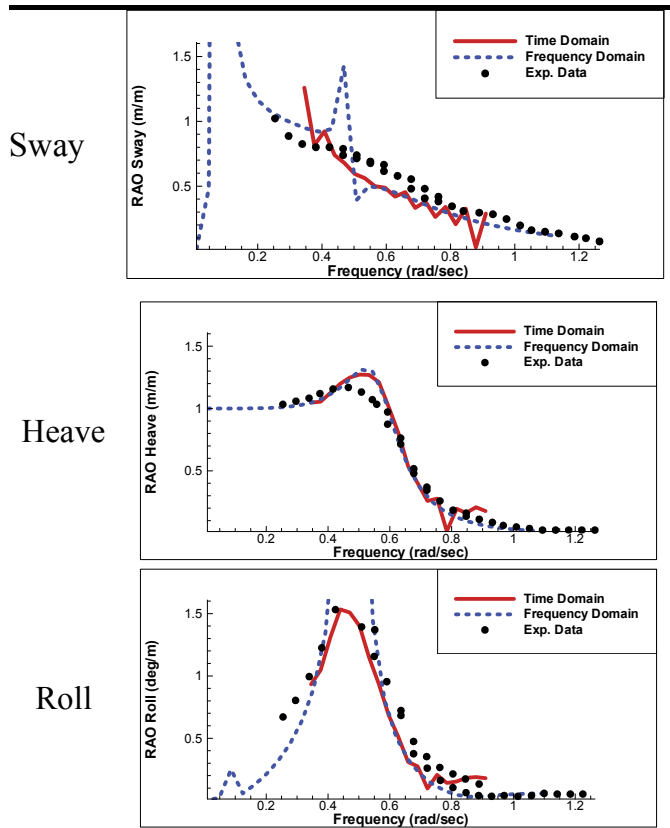


Figure 5: Comparison of simulated and measured RAOs without inner liquids.

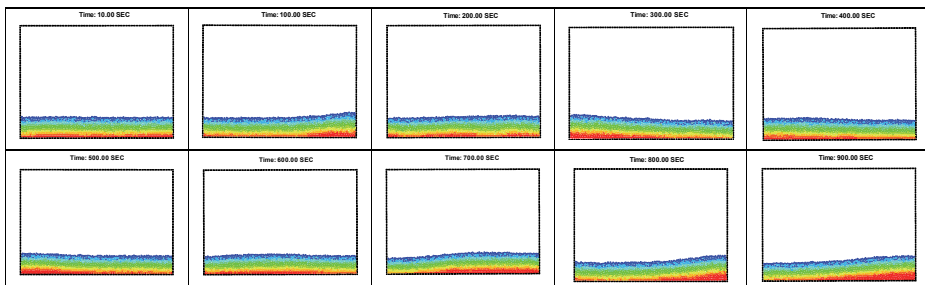


Figure 6: Snapshots of liquid motions and pressure field inside a 18% filled tank

Table 2: Characteristics of sloshing tanks.

Designation Magnitude	
AFT TANK	
Tank aft from aft perpendicular	61.08 m
Tank bottom from keel line	3.3 m
Tank length	49.68 m
Tank breadth	46.92 m
Tank height	32.23 m
FORWARD TANK	
Tank aft from aft perpendicular	209.54 m
Tank bottom from keel line	3.3 m
Tank length	56.616 m
Tank breadth	46.92 m
Tank height	32.23 m

Table 3: Principal particulars of FPSO (bare hull) and mooring system.

Description	Magnitude	
Length Between Perpendicular	285.0 m	
Breadth	63.0 m	
Draught	13.0 m	
VCG (From the Keel)	16.71 m	
Mass radius of gyration around X-axis	19.49 m	
Mass radius of gyration around Y-axis	78.42 m	
Mass radius of gyration around Z-axis	71.25 m	
Mooring Stiffness	Surge	$6.50 \times 10^5$ N/m
	Sway	$2.43 \times 10^6$ N/m
	Yaw	$1.76 \times 10^8$ Nm/rad

on the SURF scheme under the assumption that the free-surface profile is limited to single-valued function i.e. it cannot simulate very violent free-surface motions including overturning and splashing. As sloshing motions become more violent, there may be appreciable differences between the two CFD programs PNU-MPS and ABSLO3D. It needs to be also mentioned that in the case of grid-based CFD program like ABSLO3D, the mass conservation is less perfect as time increases and the accuracy of the impact-like loading is diminished because of the imposed limitations. In Fig.7, the comparisons between the two CFD programs are shown for two different  $H_s=5\text{m}$  and  $10\text{m}$ . Although both CFD programs produce similar

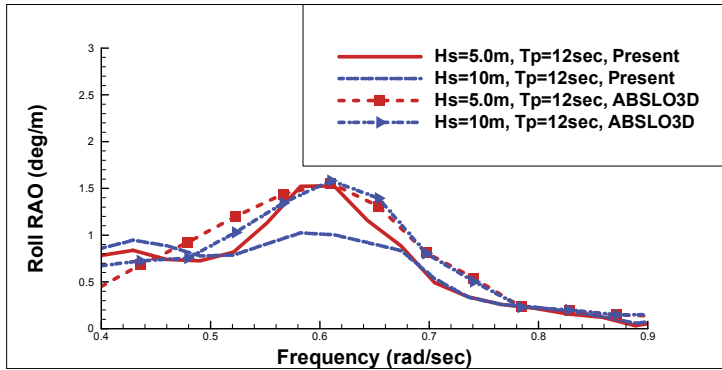


Figure 7: Motion-sloshing coupling effect of MARIN FPSO in roll. (Wave heading=90deg; filling level=18% for Hs=5m and 10m; Tp=12s)

trends, their differences are more appreciable in higher wave conditions because of the reason explained in the above.

The roll RAOs are actually very sensitive to the amount of liquid cargo and their amplitudes can be increased by a factor of 2 or 3 in some wave frequency range compared to the bare-hull case, which shows that the motion-sloshing coupling effect is actually very important. The presence of the liquid-cargo also alters the original natural frequencies of the ships with dry tanks. For example, the bare-hull roll natural frequency is 0.49rad/s, while the hull with 37% fill ratio has two natural frequencies, 0.4rad/s and 0.72rad/s. This effect is clearly demonstrated in the given simulation results. As a reference, the two lowest natural frequencies of liquid sloshing motions for various fill ratios are given in Tab.4. The analytic results are based on the linear potential theory.

Table 4: Natural frequencies of FPSO and sloshing tanks.

Bare Hull		Transverse Mode	
		Roll: 0.50	
		1 <sup>st</sup>	2 <sup>nd</sup>
Sloshing Tanks	FL: 18%	0.49	1.31
	FL: 37%	0.66	1.55
	FL: 56%	0.74	1.61

Next, let us introduce the case of larger incident waves and ship motions, and consequently, more violent sloshing motions to have an idea of nonlinear effects. For

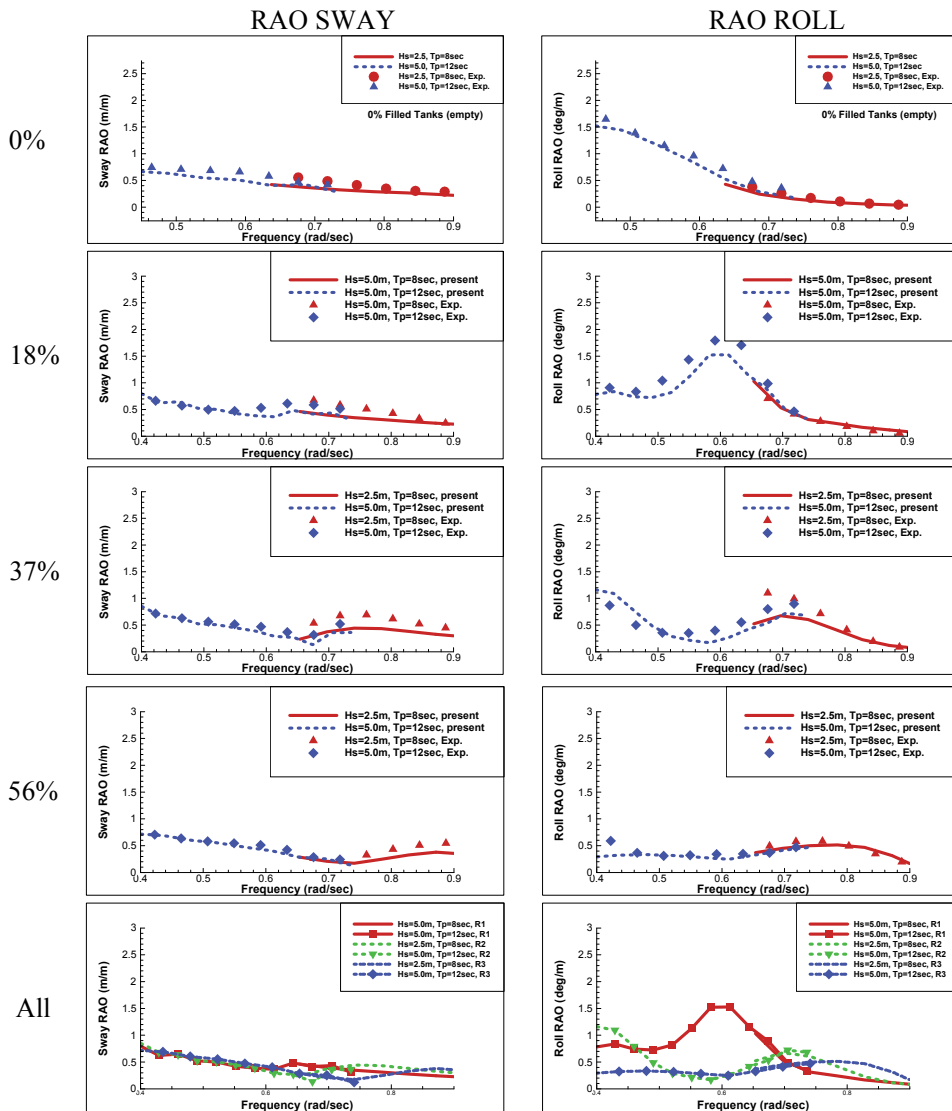


Figure 8: Simulated and measured RAOs of MARIN-FPSO for various filling ratios

this purpose, the 18% and 56% cases are selected and presented in Fig.9. The roll RAOs for 56% fill ratio are less variant with increasing Hs compared to those of 18% fill ratio, which is due to the less violent liquid sloshing motions or smaller nonlinearities in the case. Another factor is that the lowest sloshing natural frequency (0.49 rad/s) of the 18% case given in Table 5 is closer to the peak frequency

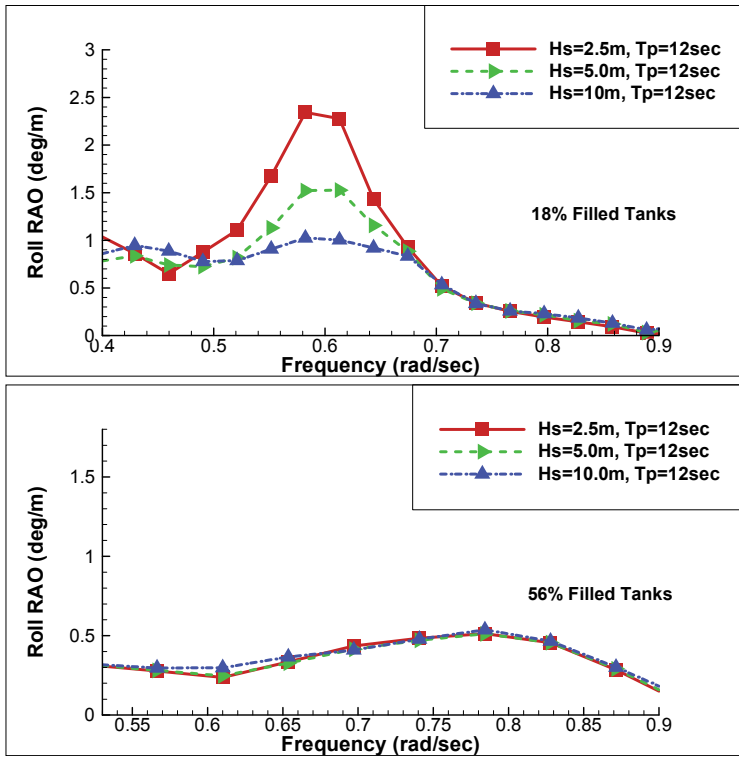


Figure 9: Comparisons of Roll RAOs for  $H_s=2.5\text{m}$ ,  $5.0\text{m}$ , and  $10\text{m}$  ( $T_p=12\text{s}$ ;  $0.52\text{ rad/s}$ )

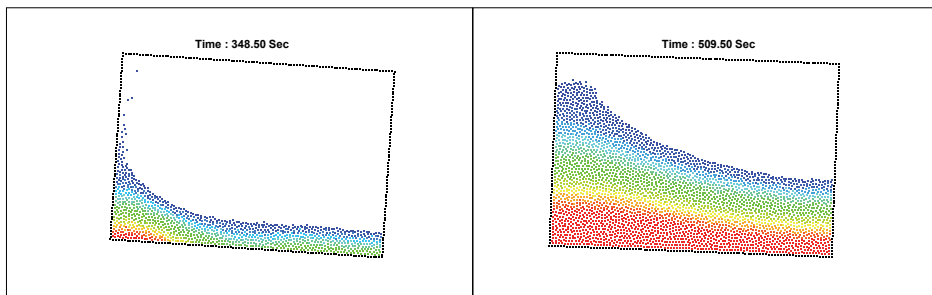


Figure 10: Representative nonlinear snapshots for inner liquid of 18% and 56% filled tank with  $H_s=5\text{m}$  and  $T_p=12\text{s}$ .

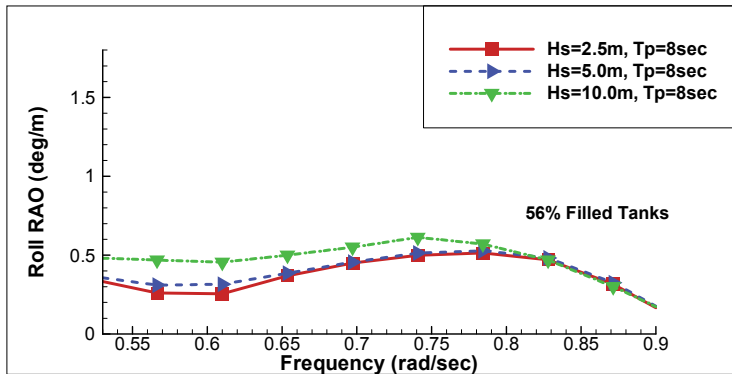


Figure 11: Comparisons of Roll RAOs for  $H_s=2.5\text{m}$ ,  $5.0\text{m}$ , and  $10\text{m}$  ( $T_p=8\text{s}$ ;  $0.78\text{ rad/s}$ )

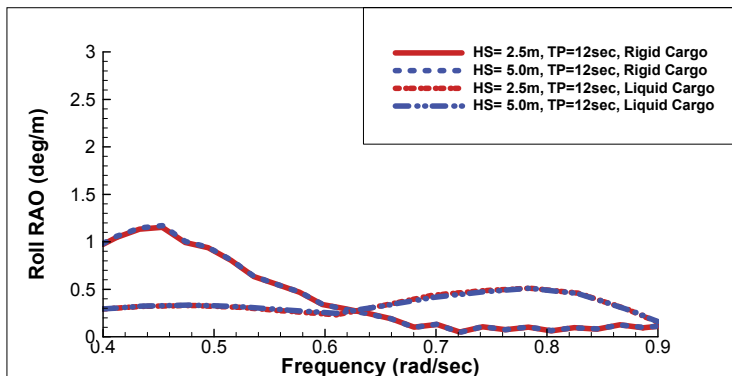


Figure 12: Comparisons of Roll RAOs between liquid and rigid cargos.

( $0.52\text{ rad/s}$ ) of the input spectrum than that ( $0.74\text{ rad/s}$ ) of the 56% case. Figure 10 shows representative nonlinear free-surface snapshots for both cases. We can see that the liquid sloshing motions become more nonlinear in 18% case. Due to the nonlinear free-surface effects, more changes of RAOs are expected in much higher waves.

Fig.11 shows the similar case of Fig.9 for 56% fill ratio but the peak period of the input spectrum is changed from 12s to 8s. The new peak frequency ( $0.78\text{ rad/s}$ ) is closer to the lowest sloshing natural frequencies ( $0.74\text{ rad/s}$ ) at that fill ratio, which means that there is more incident wave energy that can excite resonant sloshing motions inside liquid tanks. As a result, larger sloshing motions are generated and

we can see more nonlinear effects compared to Fig.9.

### **5.3 Ship Motions with Rigid Cover Inside Liquid Tanks.**

In order to investigate sloshing effects more clearly, let us consider a special case in which the free-surface is covered by a rigid cover of the same density as the water. This is exactly the case that the liquid-sloshing effects are neglected and only the total mass is increased by the amount of liquid in the vessel motion analysis i.e. the liquid cargo is treated as rigid cargo. This is the simplest approximation one can use without more sophisticated coupling programs. For the simulation of this case by PNU-MPS, the three layers of the free-surface particles are treated as rigid particles rigidly connected to the tank walls. In this case, the feedback forces and moments from sloshing tanks are only inertia forces and moments without any pressure feedback from the tank wall. Fig. 12 shows the comparisons of roll RAOs for 56% fill ratio. It is clearly seen that there exist significant differences between the rigid- and liquid-cargo cases. From the above comparisons, it can be concluded that proper vessel-motion/liquid-sloshing coupled dynamics program need to be used to accurately predict the vessel motions with sloshing effects.

## **6 Conclusions**

The liquid sloshing simulations and its interaction effects with ship motions are investigated by successfully coupling the PNU-MPS program for liquid sloshing simulation and the CHARM3D time-domain program for vessel-motion simulation. Before coupling the two programs, the reliability of each program is fully verified against respective experimental results. The ship-motion program is based on potential theory and boundary element method (3D diffraction/radiation panel method) with the correction of hull viscous drag forces. The sloshing program is based on a newly developed PNU-MPS method, which contains many features of advancement compared to the original MPS method. Then, the two programs are coupled to exchange respective data at each time step. The simulation results with the coupled dynamic analysis for various fill ratios of liquid cargo are compared with the corresponding experimental results conducted by MARIN. The predicted results correlate well against measured data for both sway and roll amplitudes. It is seen both in prediction and experiment that the roll RAOs are sensitive to the amount of liquid cargo and can be increased by a factor of 2 or 3 in some wave frequency range compared to the bare-hull case. It is also clearly demonstrated that the nonlinear sloshing effects can alter the RAOs in relatively high waves with peak period near the sloshing natural frequencies. In this regard, the developed liquid-sloshing/vessel-motion coupled dynamic analysis program can be used for the reliable prediction of vessel motions for various environmental conditions and

fill ratios of liquid cargo. The maximum sloshing impact loads can also be directly obtained during the simulation, which is very important in the design of tank walls. In order to see the influence of liquid cargo and its sloshing more clearly, the case is compared with the case with fixed cover on the free-surface i.e. the case of rigid cargo of the same mass. The comparison clearly demonstrates the need of reliable vessel-motion/liquid-sloshing coupled dynamic analysis programs.

## References

- Blackman, R. B.; Turkey, J. W.** (1958): The measurement of power spectra from the point of view of communications engineering, *Bell system Technical Journal*, vol. 37, pp. 185-282
- Cho, S.; Hong, S.Y.; Kim, J.; Park, I.** (2007): Studies on the Coupled Dynamics of Ship Motion and Sloshing including Multi-body Interactions, *Proceedings of the Seventeenth International Offshore and Polar Engineering Conference*, Lisbon, Portugal
- Faltinsen, O.M.** (1990 ): *Sea loads on ships and offshore structures*, Cambridge Press
- Gaillarde, G.; Ledoux, A.; Lynch, M.** (2004): Coupling between liquefied gas and vessel's motion for partially filled tanks, *Effect on seakeeping. Design & Operation of Gas Carriers*, RINA, London, UK.
- Gotoh, H.** (2009): Lagrangian Particle Method-Advanced Technology for Numerical Wave Flume, *Proc. 19<sup>th</sup> International Offshore and Polar Engineer Conference*, Osaka, Japan, pp. 333-339.
- Hwang S.C.; Lee B.H.; Park J.C.** (2010): Improvement of MPS Method in Simulation Violent Free-surface Motion, *Journal of Korean Society of Computational Fluids Engineering*, vol. 15, no. 1, pp. 71-80
- Kim, M.H.; Zhang, Z.** (2009): Transient effects of tendon disconnection on the survivability of a TLP in moderate-strength hurricane conditions, *Intl. Journal Naval Architecture and Ocean Engineering*, Vol.1, p13-19
- Kim, M.H.; Koo, B.J.; Mercier, R.M.; Ward, E.G.** (2005): Vessel/mooring/riser coupled dynamic analysis of a turret-moored FPSO compared with OTRC experiment, *Journal of Ocean Engineering* Vol.32, 1780-1802
- Kim, M.H.; Ran, Z.; Zheng, W.** (2001): Hull/mooring coupled dynamic analysis of a truss spar in time domain, *Journal of Offshore and Polar Engineering*, Vol.11, No.1, 42-54
- Kim, Y.; Shin, Y.; Kin, W.; Yue. D.** (2003): Study on Sloshing Problem Coupled with Ship Motion in Waves, *The 8th International Conference on Numerical Ship*

*Hydrodynamics*, Busan, Korea

**Kim, Y.; Nam, B.W.; Kim, D.W.; Kim, Y.S.** (2007): Study on Coupling Effect of Ship Motion and Sloshing, *Ocean Engineering*, vol. 34, pp. 2176-2178.

**Kishev, Z.; Hu, C.; Kashiwagi, M.** (2006): Numerical simulation of violent sloshing by a CIP-based method, *J. Mar Sci Techol*, vol. 11, pp. 111-122.

**Koo, B.J. and Kim, M.H.** (2005): Hydrodynamic Interactions and Relative Motions of Two Floating Platforms with Mooring Lines in Side-by-side Offloading Operation, *Journal of Applied Ocean Research*, Vol.27 #6, 295-310

**Koshizuka, S.; Tamako, H.; Oka, Y.** (1996): Moving-Particle semi-implicit method for fragmentation of incompressible fluid. *Numerical science and Engineering*, vol. 123, pp. 421-434

**Lee, B.H.; Park, J.C.; Kim, M.H.** (2010): Numerical simulation of impact loads using a particle method, *Ocean Engineering*, vol.37, pp.164-173

**Lee, B.H., Park, J.C., and Kim, M.H.** (2011): Step-by-step improvement of MPS method in simulating violent free-surface motions and impact loads, *J. Computer Methods in Applied Mechanics and Engineering*, Vol.200 1113-1125

**Lee, C.H.** (1995): *WAMIT Theory Manual: MIT Report 95-2*, Dept. of Ocean engineering, Massachusetts Institute of Technology, Cambridge, MA.

**Lee, C.H.; Newman, J.N.; Kim, M.H.; Yue, D.K.P.** (1991): The computation of second-order wave loads, *Proc. 10th International Conf. OMAE*, Stavanger, Norway

**Lee S.J.; Kim M.H.; Lee, D.H.; Kim, J.W.; Kim, Y.H.** (2007): The effects of LNG-tank sloshing on the global motions of LNG carriers, *J. of Ocean Engineering*, Vol.34 #1 pp.3-9

**Lee, S.J. and Kim, M.H.** (2008): The effects of tank sloshing on LNG vessel and floating terminal responses, *Proc. 27th Int. Offshore Mechanics and Arctic Eng. Conference*, Lisbon

**Lee, S.J. and Kim, M.H.** (2010): The effects of inner liquid motion on LNG vessel responses, *J. of Offshore Mechanics and Arctic Engineering*, Vol.132 #2

**Toyota, E., Akimoto, H. and Kubo, S.** (2005): A particle method with variable spatial resolution for incompressible flows, *19<sup>th</sup> Japan Society of Fluid Mechanics*, A9-2.

